Pulsed Field Ionization Electron Spectroscopy and Molecular Structure of Aluminum Uracil

Serge A. Krasnokutski and Dong-Sheng Yang*

Department of Chemistry, University of Kentucky, Lexington, Kentucky 40506-0055

Received: June 25, 2007; In Final Form: August 9, 2007

Al−uracil (Al−$C_4H_4N_2O_2$) was synthesized in a laser-vaporization supersonic molecular beam source and studied with pulsed field ionization−zero electron kinetic energy (ZEKE) photoelectron spectroscopy and density functional theory (DFT). The DFT calculations predicted several low-energy Al−uracil isomers with Al binding to the diketo, keto−enol, and dienol tautomers of uracil. The ZEKE spectroscopic measurements of Al−uracil determined the ionization energy of 43 064(5) cm^{-1} [or 5.340(6) eV] and a vibrational mode of 51 cm^{-1} for the neutral complex and several vibrational modes of 51, 303, 614, and 739 cm^{-1} for the ionized species. Combination of the ZEEK spectrum with the DFT and Franck−Condon factor calculations determined the preferred isomeric structure and electronic states of the Al−uracil complex. This isomer is formed by Al binding to the O4 atom of the diketo tautomer of uracil and has a planar C_s symmetry. The ground electronic states of the neutral and ionized species are $^2A''$ and $^1A'$, respectively. The $^2A''$ neutral state has a slightly shorter Al−O4 distance than the $^1A'$ ion state. However, the $^1A'$ ion state has stronger metal−ligand binding compared to the $^2A''$ state. The increased Al−O4 distance from the $^2A''$ state to the $^1A'$ state is attributed to the loss of the π binding interaction between Al and O4 in the singlet ion state, whereas the increased metal−ligand binding strength is due to the additional charge−dipole interaction in the ion that surpasses the loss of the π orbital interaction.

1. Introduction

Metal coordination with DNA and RNA bases may change the course of genetic information transfer by disrupting hydrogen bonding in base pairs.[1−5] On the other hand, introduction of metal-induced base pairs into DNA can create self-assembled nanoscale arrays with distinct structures and functions.[6−8] In these systems, metal binding sites, bond strengths, and bonding mechanisms influence the structures and properties of the nucleic acids.[9]

Recently, several research groups reported studies of these nucleobases bound to metal ions and atoms in the gas-phase environment, where complications from solvent molecules and counterions were removed. Cerda and Wesdemiotis determined alkali metal ion ($M^+ = Li^+$, Na^+, K^+) affinities of the DNA and RNA bases by investigating the dissociation of metal ion-bound heterodimers and discussed possible ion binding sites based on the observed entropy changes and ion affinities.[10] Rodgers and Armentrout studied threshold collision-induced dissociation of M^+L ($M^+ = Li^+$, Na^+, and K^+; L = uracil, thymine, and adenine) and M^+(adenine) (M = Sc^+, Ti^+, V^+, Cr^+, Mn^+, Fe^+, Co^+, Ni^+, Cu^+, and Zn^+) using guided ion beam mass spectrometry.[11,12] In combination with theoretical calculations, they examined the preferred binding sites of alkali, early transition, and late transition elements. Following these studies, Yang and Rodgers studied the threshold collision-induced dissociation of alkali ion complexes with substituted uracils and found that methalation, halogenation, thio substitution, or combination of these effects did not influence binding energies significantly or change the binding sites of the alkali ions.[13−15] Using laser photodissociation, Yang and co-workers measured photofragmentation spectra of $Mg^+−L$ (L = uracil, thymine, and cytosine) and detected the dissociation products of the metal

ion and organic fragments.[16,17] For nucleobase complexes with neutral metal atoms, Pedersen and co-workers measured photoionization efficiency (PIE) spectra of Al−cytosine and Al−guanine−$(NH_3)_{0−2}$ and studied photoinduced dehydrogenation of Al−L (L = cytosine, guanine, and guanine−cytosine).[18−20] In these studies, the authors observed that the photophysics of the gas-phase complexes was similar to that of solution-phase bases.

In addition to these experimental measurements, theoretical calculations have been reported on the binding sites and energies of cations[11,12,21−25] and structures and ionization energies of neutral complexes.[26−29] In binding with metal atoms or ions, nucleobases can function as σ or π ligands, but their σ binding is often stronger than π binding. From previous density functional theory (DFT) calculations, low-energy sites for cation (Li^+, Na^+, K^+, and Cu^+) coordination were mainly the N3 and O2 atoms of cytosine, O4 and O2 atoms of uracil and thymine, N9, N7, N6, and N3 atoms of adenine, and N9, N7, O6, and N3 atoms of guanine.[21,22] However, the preferred binding sites of adenine from the DFT calculations were not consistent with those from Møller−Plesset (MP2) theory, where the low-energy sites were predicted to be N7, N3, and N1.[11,12] For neutral metal atoms (Al and Cu), the binding sites were similar to those of the cations, but the relative stability of low-energy isomers was different from that of cations.[26] The challenge in determining the structures of metal−nucleobase complexes is due to small energy differences between low-energy isomers. These differences are often within computational errors such that theory alone is unable to identify preferred binding sites. For example, the energy differences predicted by the DFT calculations were only 1.7 kcal mol^{-1} between O4- and O2-bound Cu−uracil and 0.3 kcal mol^{-1} between N9- and N3-bound Cu−guanine.[26]

In this study, we report the first electronic−vibrational spectroscopy and the molecular structure of Al−uracil. The

---

* Corresponding author. E-mail: dyang0@uky.edu.

electronic–vibrational spectrum was measured with pulsed field ionization–zero electron kinetic energy (ZEKE) spectroscopy, and the preferred Al binding site was determined by combining the spectroscopic measurements with theoretical calculations.

2. Experimental and Computational Methods

The experimental setup has been described in a previous publication.[30] Al–uracil was prepared by reactions of Al atoms and uracil molecules in a pulsed molecular beam source. The Al atoms and uracil molecules were produced by laser ablation of a rod made of Al (Aldrich, 99%, −200 meshes) and uracil (Alfa Aesar, 99%) powders. The vaporization was carried out with the second-harmonic output of a Nd:YAG laser (Quanta-Ray, GCR-3, 532 nm, 15 mJ) in the presence of He carrier gas (UHP, Scott-Gross) with a stagnation pressure of 35 psi. The vaporization laser was focused by a plano–convex lens with a 30 cm focal length. The carrier gas was delivered by a homemade piezoelectric pulsed valve.[31] The ablation rod was translated and rotated by a motor-driven mechanism to ensure that each laser pulse ablated a fresh surface. The complex was identified by photoionization time-of-flight mass spectrometry, and its first ionization threshold was located by recording the mass-selected ion signal as a function of ionization laser wavelength. Prior to the ZEKE experiment, the production of the Al–uracil complex was maximized by adjusting the timing and power of the vaporization and ionization lasers and reservoir pressure of the carrier gas. ZEKE electrons were produced by photoexcitation of neutral molecules to highly excited Rydberg states, followed by pulsed electric field ionization (1.1 V cm^{-1}, 100 ns) of these Rydberg states. A small dc field of 0.08 V/cm was applied to remove kinetic electrons produced by direct photoionization. The photoionization and photoexcitation light was provided by a frequency-doubled dye laser (Lumonics HD-500), pumped by the third-harmonic output of a second Nd:YAG laser (Continuum, Surelite II, 355 nm). The pulsed electric field was generated by a delay pulse generator (Stanford Research System, DG535). The ion and electron signals were detected by a dual-microchannel plate detector (Galileo), amplified by a preamplifier (Stanford Research System, SR445), averaged by a gated integrator (Stanford Research System, SR250). Laser wavelengths were calibrated against vanadium atomic transitions.[32] Field-dependent measurements were not performed due to the limited size of the ZEKE signal. However, the energy shift caused by the pulsed field (1.1 V cm^{-1}) is expected to be smaller than the spectral line width (full width at half-maximum height).[33]

Geometry optimization and vibrational analysis were carried out with the hybrid B3P86 DFT method and the 6-311+G(d,p) basis implemented in GAUSSIAN 03.[34] Multidimensional Franck–Condon (FC) factors were calculated from the theoretical equilibrium geometries, harmonic vibrational frequencies, and normal coordinates of the neutral and ionic complexes.[35,36] The Duschinsky effect[37] was considered to account for normal mode differences between the neutral and ion complexes in the FC calculations. Spectral broadening was simulated by giving each line a Lorentzian line shape with the line width of the experimental spectrum. Boltzmann distributions were used to simulate spectra at specific temperatures.

3. Results and Discussion

3.A. Low-Energy Isomers of Al–Uracil. Like other nucleobases, uracil may exist in different tautomeric forms that result from hydrogen migration in the molecule. Previously, ab initio calculations predicted 13 low-energy tautomers of uracil in

diketo, keto–enol, and dienol forms,[38,39] and the most stable tautomer was determined to be the diketo form (2,4-dioxopyrimidine) by both the theoretical calculations[38,39] and spectroscopic measurements.[40–42] In our experiment, uracil was vaporized by laser ablation; this ablation process may generate uracil molecules in both the canonical and noncanonical forms that can interact with metal atoms. Moreover, metal coordination has been found to influence the tautomeric equilibrium of nucleobases and thus their relative abundances.[43] Therefore, in our computational survey of Al–uracil isomers, we have considered diketo, keto–enol, and dienol forms of uracil, which are shown in the middle column of Figure 1. Consistent with the previous ab initio calculations, our DFT calculations predict the diketo tautomer to be the most stable form and the keto–enol (N1O2, N3O4, N3O2, N1O4) and dienol (N1O2N3O4) tautomers to be the less stable form with energy up to about 22 kcal mol^{-1} above the diketo tautomer. The less stable tautomers are formed by hydrogen migration from the NH groups to the oxygen atoms in the canonical diketo form. For example, the N1O2 keto–enol tautomer is formed by a hydrogen transfer from the N1 position to the O2 position, whereas the N1O2N3O4 dienol tautomer is formed by hydrogen transfer from N1 and N3 to O2 and O4, respectively. Although each noncanonical tautomer has one or more rotational conformers as predicted by previous calculations,[38,39] only the most stable one is considered in Figure 1. Among these noncanonical tautomers, our calculations show that the most stable structures are formed with hydrogen migration to the nearest oxygen atom and have an intramolecular hydrogen bond (O–H···N).

Al–uracil complex can be formed by σ binding to the oxygen or nitrogen atoms or by π binding on the top of the aromatic ring of uracil. In either case, the ground electronic state of the complex is a doublet state arising from the interaction between the doublet Al atom (^{2}P, 3p^1) and singlet uracil molecule. The σ structures of the neutral complex have the Al atom in the same plane as the uracil ring atoms and are presented with their relative energies on the left side of Figure 1. As for the free ligand, Figure 1 presents only the most stable rotational conformer for each Al–uracil isomer. The canonical uracil has two oxygen binding sites and forms two Al–uracil isomers by Al binding to the O4 and O2 positions, respectively. The Al–O4 isomer is 18.2 kcal mol^{-1} more stable than Al–O2. The O4 site is more favorable than O2 because the former allows the Al–O4 bond to align better with the electric dipole of the canonic uracil molecule. For noncanonical uracil tautomers, the N3O4, N3O2, and N1O4 keto–enol forms have adjacent oxygen and nitrogen atoms that are not bound to hydrogen and can provide two binding sites for Al coordination. On the other hand, the N1O2 keto–enol and N1O2N3O4 dienol tautomers contain no such neighboring oxygen or nitrogen atoms and have a single binding site for Al. As a result, the Al–N3O4, Al–N1O4, and Al–N3O2 isomers are more stable than the Al–N1O2 and Al–N1O2N3O4 isomers. Because Al binding modes (mono- or bidentate) are different in these noncanonical tautomers, coordination of an Al atom has changed the order of their relative stabilities. The relative energies follow the order of N1O2 < N3O4 < N1O2N3O4 < N3O2 < N1O4 in the free ligand, whereas this energy order is changed to N3O4 < N1O4 < N3O2 < N1O2 < N1O2N3O4 upon metal coordination. However, the Al–uracil isomers formed with these noncanonical tautomers are still less stable than those formed with the canonical diketo form. Additionally, we have estimated the binding energy difference of about 8 kcal mol^{-1} between the Al–O and Al–N bonds by considering the energy differences between Al–N1O2

Spectroscopy and Structure of Aluminum Uracil

J. Phys. Chem. A, Vol. 111, No. 42, 2007 **10569**
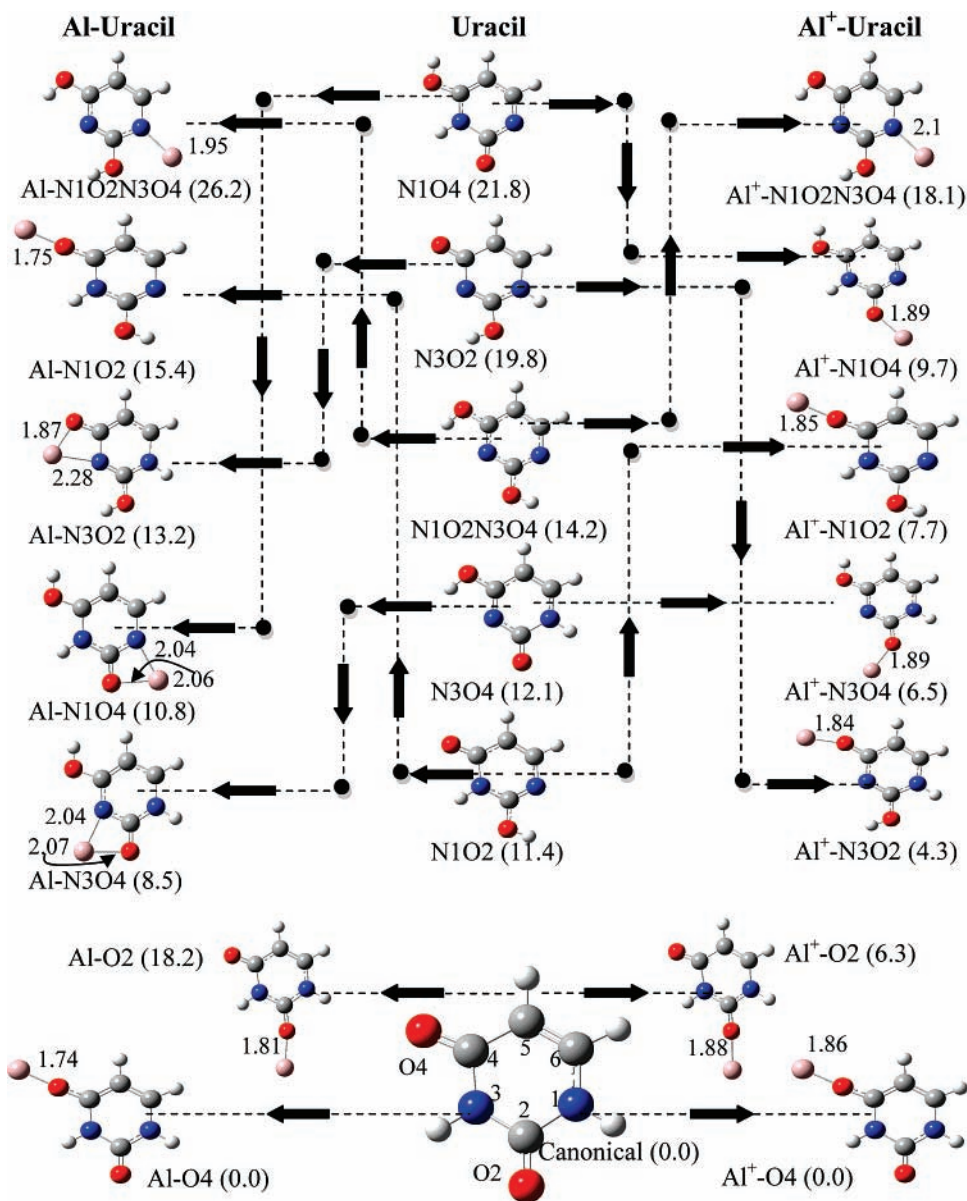
Figure 1. Low-energy tautomers of uracil (middle column) and isomers of Al−uracil (left column) and Al+−uracil (right column) obtained from B3P86/6-311+G(d, p) calculations. Bond distances are in angstroms, and relative energies inside parentheses are in kcal mol⁻¹.

and Al−N1O2N3O4 and between N1O2 and N1O2N3O4. This estimation shows that oxygen atoms are better σ binding sites than the nitrogen atoms for Al coordination, similar to a previous prediction for Cu−uracil.[26] For Al π binding, our calculations predict a π structure with Al binding above the C5−C6 double bond and 23.4 kcal mol⁻¹ higher in energy than the Al−O4 σ structure.

The σ structures and relative energies of Al+−uracil are shown on the right side of Figure 1. Like the neutral isomers, the ionic isomers have Al+ in the same plane as the uracil ring atoms; the Al+−O4 isomer is more stable than the Al+−O2 and Al+-noncanonical isomers; Al+−O binding is stronger than Al+−N; and the ions formed with the keto−enol tautomers (N3O2, N1O2, N3O4, and N1O4) are more stable than that with the dienol tautomer (N1O2N3O4). However, a number of significant differences exist between the neutral and ionic isomers. The energy difference between the Al−O4 and Al−O2 structures is decreased from 18.2 kcal mol⁻¹ in the neutral state to 6.3 kcal mol⁻¹ in the ionic state; the bidentate Al binding with the keto−enol N3O4, N1O4, and N3O2 isomers becomes monodentate upon ionization, the relative stability of the Al+-

bound noncanonical tautomers is different from that of the corresponding neutral complexes, and the energy differences between the Al+-bound noncanonical and canonical uracil tautomers are much smaller than those in their neutral counterparts. Moreover, no minimum energy π structure was located for the ion; the π structure of the ionized complex was converged to the most stable Al+−O4 σ ion structure. All these differences can be attributed to the charge−dipole interaction in the ion, which not only enhances the metal−ligand binding but also dictates the structures of the ion isomers. For example, Al+−N3O2 is more stable than all other Al+-noncanonical−uracil isomers because the N3O2 tautomer has a large electric dipole with its direction approximately aligned with the Al+−O4 bond.[39]

As discussed above, Al or Al+ coordination changes the relative stability of the uracil tautomers and, thus, their populations at ambient temperatures. For example, the energy difference between the canonical form and the lowest-energy noncanonical N1O2 tautomer of the free uracil is predicted to be 11.4 kcal mol⁻¹, whereas the energy differences is reduced to 8.5 kcal mol⁻¹ between the most stable Al-canonical (Al−
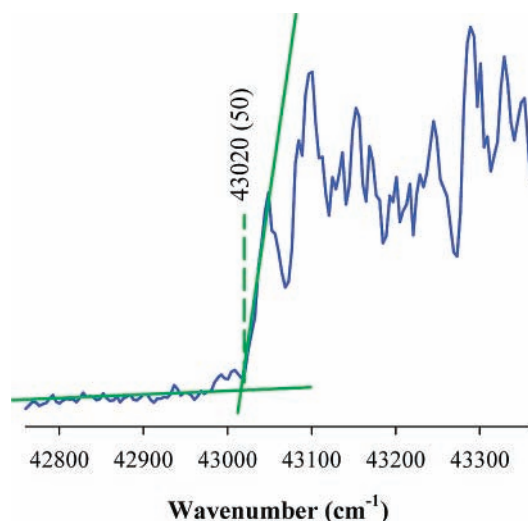
Figure 2. Photoionization efficiency spectrum of Al−uracil seeded in He carrier gas. The position of the ion signal onset at 43 020(50) cm^{-1} indicates approximate ionization energy (IE) of the complex.

O4) and Al-noncanonical (Al−N3O4) neutral isomers and 4.3 kcal mol^{-1} between the most stable Al$^+$-canonical (Al$^+$−O4) and Al-noncanonical (Al$^+$−N3O2) isomeric ions. Using the simple thermodynamic equation $\eta_1/\eta_2 = \exp(-\Delta G_{12}/RT)$, where η_1 and η_2 stand for the populations of the noncanonical and canonical uracil tautomers or metal-bound uracil isomers, ΔG_{12} the Gibbs free energy difference of the two species from the DFT calculations, R the gas constant, and T the temperature, we have estimated that relative population of the noncanonical tautomers versus the canonical form is increased by $\sim10^2$ times from the free ligand to the neutral Al-bound uracil and by $\sim10^5$ times to the ionic Al$^+$-bound uracil at $T = 298$ K. In this estimation, the temperature dependence of the Gibbs free energy was ignored, and only the most stable canonical and nonca-nonical forms were considered. The effect of Al coordination on the relative stability of the uracil tautomers is similar to that of microhydration and solvation.[38,39]

3.B. Spectroscopy of Al−Uracil. Figure 2 presents a representative PIE spectrum of Al−uracil seeded in helium carrier gas. The spectrum shows a clear signal onset at 43 020-(60) cm^{-1}, which corresponds to the first ionization energy (IE) of the complex. This value was obtained by locating a point at which a line drawn through the sharp signal onset interacts with a line drawn through the baseline and corrected by +110 cm^{-1} to the laser wavenumbers to account for Stark effect of the electric field (320 V cm^{-1}) presented in the ionization region. Although it has a relatively large uncertainty, the IE value measured from the PIE spectrum simplifies the ZEKE experi-ment. Moreover, such photoionization measurements in the mass-operation mode are used to correlate with the high-resolution ZEKE experiment.

Figure 3a shows the experimental ZEKE spectrum of Al−uracil seeded in He. The spectrum originates at 43 064(5) cm^{-1} with the line width of 10 cm^{-1}. At the higher energy side of the band origin (0−0), the spectrum displays vibrational intervals of 303, 614, and 739 cm^{-1}. Additionally, the spectrum exhibits 51 cm^{-1} intervals on one or both sides of the band origin and 303, 614, and 739 cm^{-1} peaks above the 0−0 transition. The intensities of the 51 cm^{-1} peaks at the lower energy side of the band origin and 303 and 614 cm^{-1} peaks depended on the molecular beam conditions and are thus attributed to transitions from excited vibrational levels of the neutral complex. By comparing with the infrared (IR) spectra of the free ligand[40−42,44,45]
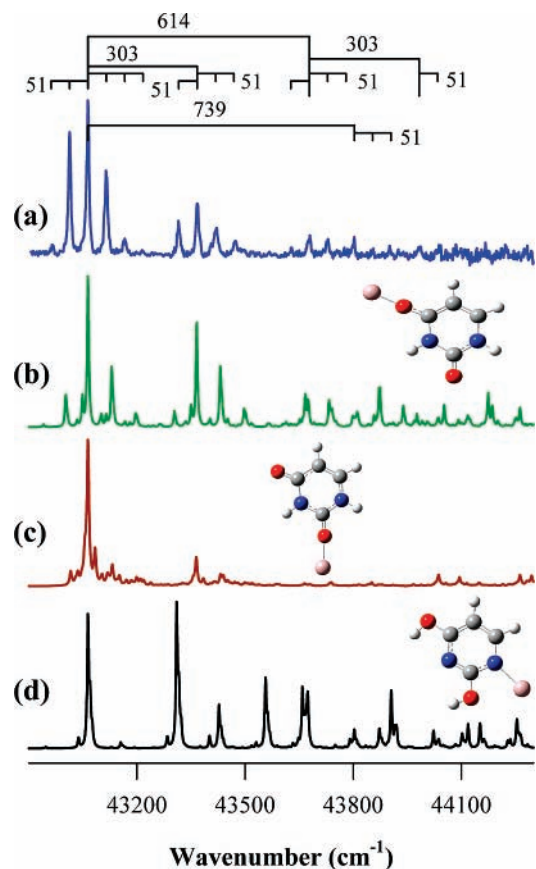
Figure 3. Experimental ZEKE spectrum of Al−uracil seeded in He (a) and simulations of Al−O4 (b), Al−O2 (c), and Al−N1O2N3O4 (d) isomers at 70 K. The neutral and ion structures of these isomers were obtained from the B3P86/6-311+G(d,p) calculations. The vibra-tional intervals in the experimental spectrum are discussed in text and identified in Table 1.

and the ZEKE spectrum of an Al−heterocyclic aromatic molecule,[46] the 614 and 739 cm^{-1} intervals are assigned to the excitations of the uracil-based vibrations, whereas the 51 and 303 cm^{-1} intervals may be attributed to Al−uracil vibrations.

Although there have been no spectroscopic studies for Al−uracil, a number of IR studies have been reported for the free ligand. Matrix isolation IR studies reported the uracil ring breathing frequencies of 780 cm^{-1} in Kr, 759 or 719 cm^{-1} in Ar, 756 cm^{-1} in Ne, and 724 cm^{-1} in N$_2$.[41,42] In the vapor phase, a weak IR peak was measured at 757 cm^{-1} for the free ligand.[40] Thus, the 739 cm^{-1} excitation in the ZEKE spectrum of Al−uracil is likely due to the uracil ring breathing vibration as well. Additionally, a number of IR transitions were reported at $\sim$650 $\pm$ 10 and 530 $\pm$ 30 cm^{-1} in both inert gas matrices[41,42] and the gas phase.[40] These transitions were attributed to ring-based bending vibrations. Hence, the 614 cm^{-1} peak in the ZEKE spectrum should be associated with one of these ring vibrations. There have been no IR transitions around 300 cm^{-1} or below reported for the ligand. Therefore, the 51 and 303 cm^{-1} intervals are likely due to the excitations of metal−ligand vibrations. The 303 cm^{-1} interval is close to the Al$^+$−imidazole stretching frequency of 313 cm^{-1} measured in the ZEKE spectrum of Al−imidazole[46] and may be attributed to the Al$^+$−uracil stretch excitation. In the following section, we will discuss further about the spectral assignments and structural identification by com-bining the spectroscopic measurements with the theoretical calculations.

Spectroscopy and Structure of Aluminum Uracil

J. Phys. Chem. A, Vol. 111, No. 42, 2007 **10571**

As discussed in section 3.A., Al binding to the canonical and noncanonical tautomers of uracil forms a number of low-energy isomers of Al−uracil (Figure 1). Among these isomers, the neutral Al−N1O2 is predicted to be a transition state with an imaginary frequency. Thus, this isomer shall not contribute to the observed spectrum. The neutral Al−N3O4, Al−N1O4, and Al−N3O2 isomers have a bidentate binding mode, whereas the binding in the corresponding ion is monodentate. The switch of the metal binding modes has caused a large geometry change from the neutral molecule to the ion, and our FC factor calculations have predicted a much longer FC profile than the experimental spectrum. Therefore, these three isomers shall not be the ZEKE spectral carriers and will be excluded from further considerations in our spectral analysis. The remaining three isomers, Al−O4, Al−O2, and Al−N1O2N3O4 have a smaller structural change upon ionization and should yield a shorter FC profile by the ionization process. Figure 3b−d exhibits the spectral simulations for these isomers. In these simulations, the calculated vibrational frequencies are not scaled, but the 0−0 transition energies are shifted to the experimental value for easier comparison with the experimental spectrum in Figure 3a. The Al−N1O2N3O4 simulation (Figure 3d) fails to reproduce the experimental 51 cm^{-1} vibrations and displays a number of strong bands that are not observed in the experiment. For the Al−O2 isomer, although its simulation shows a numbers of small peaks around the 0−0 transition, the intensities and positions of these weak peaks do not match the experimental 51 cm^{-1} vibrations. In addition, the Al−O2 simulation misses the 614 and 739 cm^{-1} intervals and their combinations with the 51 cm^{-1} transitions. On the other hand, the Al−O4 simulation (Figure 3b) shows a much better match to the experimental spectrum, although the intensities for some of higher energy transitions are somewhat overestimated. The predicted vibrational frequencies of 62/66, 302, and 612 cm^{-1} for the Al−O4 isomer are close to the measured values of 55/55, 303, and 614 cm^{-1}, respectively, and the calculated value of 739 cm^{-1} has a fair comparison to the measured 809 cm^{-1} interval as well. From these comparisons, the observed spectrum is likely due to ionization of the Al−O4 isomer. This conclusion should not be surprising since Al−O4 is predicted to be the most stable isomer of Al−uracil, and other isomers are at least 8.5 kcal mol^{-1} higher in energy. These higher-energy isomers are unlikely populated with a significant amount in the supersonic molecular beam. With the identification of the spectral carrier and the good match between the Al−O4 simulation and the experimental spectrum, spectral assignment becomes straightforward. The 51 cm^{-1} intervals at the lower energy side of the 0−0, 303, and 614 cm^{-1} peaks are assigned to the transitions from the vibrationally excited levels of an out-of-plane Al−uracil bend in the neutral state, whereas the 51 intervals at the higher energy sides of these (0−0 transition and 303 and 614 cm^{-1}) and 739 cm^{-1} peaks are due to an in-plane Al$^+$−uracil bend in the ion state. The 303, 614, and 839 cm^{-1} intervals are attributed to the excitations of the Al$^+$−uracil stretch, in-plane uracil ring deformation, and uracil ring breath vibrations in the ion state, respectively. The Al$^+$−uracil stretch is characterized by the Al$^+$ displacement, where the in-plane uracil deformation is accompanied by the displacement of the O4 atom. The assignment of the 614 and 839 cm^{-1} to the uracil-based vibrations is consistent with that obtained by comparing the ZEKE spectrum of Al−uracil with the IR spectra of the free ligand. The complete assignment for each observed transition is summarized in Table 1. This table also compares the experimental and theoretical IE and vibrational frequencies. The calculated frequencies, especially for the Al$^+$−

TABLE 1: ZEKE Peak Positions (cm^{-1}) and Assignments of Al−Uracil[a]

ZEKE (0 = 43064)	assignment	B3P86/6-311+G(d,p) (0 = 47844)	vibrations[b]
−98	23_2^0		
−51	23_1^0	−62	Al−uracil o.p. bend
0	0_0^0	0	
51	23_0^1	66	Al$^+$−uracil i.p. bend
102	23_0^2		
251	$23_1^0 22_0^1$		
303	22_0^1	302	Al$^+$−uracil stretch
355	$22_0^1 23_0^1$		
409	$22_0^1 23_0^2$		
565	$23_1^0 20_0^1$		
614	18_0^1	612	uracil ring i.p. deformation
665	$18_0^1 23_0^1$		
739	17_0^1	809	uracil ring breath
789	$17_0^1 23_0^1$		
838	$17_0^1 23_0^1$		
919	$18_0^1 22_0^2$		
972	$18_0^1 22_0^1 23_0^1$		

[a] The uncertainty of the peak positions: 5 cm^{-1}. [b] o.p., out-of-plane; i.p., in-plane.

uracil stretch and uracil ring deformation, are in very good agreement with the measured values. The predicted IE is, however, about 0.6 eV higher than the experimental value. Similar IE overestimates by the B3P86 hybrid functional have also been found for other metal-containing molecules.[36,47−49]

3.C. Structure and Bonding of the Observed Al−Uracil Isomer. The most stable structure of Al−uracil determined by the combination of the experiment and theory has C_s symmetry, where Al atom binds to the O4 atom and is in the same plane as that of the uracil ring atoms. This structure is different from the nonplanar Cu−uracil.[26] The ground electronic state of the neutral molecule is $^2A''$ and that of the corresponding ion is $^1A'$. The major differences between the $^2A''$ and $^1A'$ states are in the Al−O distance and Al−O4−C4 angle. The Al−O distance increases from 1.74 in the $^2A''$ state to 1.86 Å in the $^1A'$ state, and the Al−O4−C4 angle decreases from 176° to 171°. These major geometry changes are confirmed by the ZEKE spectrum, which shows a strong FC activity for both the Al−O stretching and Al−uracil bending vibrations. In general, metal−ligand distances of weakly bound association complexes shrink upon ionization and the resulting metal ion−ligand bonding is stronger due to the additional charge−dipole interaction in the ionized complex. In Al−uracil, the Al$^+$ binding is also stronger as indicated by the IE value of the complex. The IE of Al−uracil is measured to be 43 064(5) cm^{-1} [or 5.340(6) eV], which is 4674 cm^{-1} lower than that of Al atom.[50] The IE red shift from Al to Al−uracil equals the dissociation energy difference between Al$^+$−uracil and Al−uracil. At first glance, the increase of the metal ion−ligand binding strength contradicts to the predicted increase of the Al−uracil distance upon ionization. The major reason for this seemly inconsistency is due to the removal of a π bonding electron from the highest occupied molecular orbital (HOMO) of Al−uracil by ionization. It can be seen from Figure 4 that an Al 3p electron is perpendicular to the molecular plane and overlaps with an O4

Krasnokutski and Yang
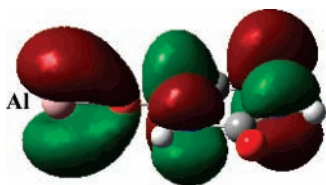
Figure 4. Electron density map of the highest occupied molecular orbital (HOMO) of the Al—O4 isomer obtained from the B3P86/6-311+G(d,p) calculations. The figure shows π bonding between Al 3p and O4 2p orbitals and π antibonding among C 2p and N 2p orbitals of the uracil ring atoms.

2p electron in an in-phase π fashion. Ionization removes this Al—O4 π bonding and thus increases the Al—uracil distance. However, the loss of the π bonding is more than offset by the additional charge—dipole interaction in the ion. Therefore, the Al$^+$ ion binding is still stronger than the corresponding neutral bonding.

4. Conclusions

In this article, we have reported the first joint electronic—vibrational spectroscopic and computational study of Al—uracil. The low-energy tautomers of isolated uracil includes the diketo, keto—enol, and dienol forms, with the keto tautomers having the lowest energy. Al binding to these tautomers forms several low-energy isomers, and their relative energies depend on the tautomeric forms of uracil and the binding sites of Al. Among all three forms of uracil, Al binding to the diketo tautomer yields the most stable Al—uracil structure, whereas Al binding to the dienol tautomer forms the least stable structure. The relatively stability of these Al—uracil isomers is different from that of the free uracil tautomers, and metal coordination stabilizes significantly the keto—enol tautomers and destabilizes the dienol forms. For a specific tautomer, oxygen is the preferred site for Al binding. The observed Al—uracil isomer is formed by Al binding to the diketo form of uracil and corresponds to the most stable structure predicted by theory. In this structure, Al binds to the O4 atom and is in the same plane as that of the uracil molecule. Although the Al binding is largely σ character, π orbital interaction between Al and O4 also contributes to the metal—uracil binding. The IE of this Al—O4 structure is lower than that of the bare Al atom, and the Al$^+$—uracil ion binding is stronger compared to Al—uracil neutral binding due to the additional charge—dipole interaction.

References and Notes

(1) Jortner, J.; Bixon, M.; Langenbacher, T.; Michel-Beyerle, M. E. *Proc. Natl. Acad. Sci. U.S.A.* **1998**, *95*, 12859.

(2) Hall, D. B.; Holmlin, R. E.; Barton, J. K. *Nature* **1996**, *382*, 731.

(3) Lippard, S. J. *Principles of Bioinorganic Chemistry*; University Science Books: Mill Valley, CA, 1994.

(4) *Metal Ions in Biological Systems*; Sigel, A., Sigel, H., Eds.; Marcel Dekker, Inc.: New York, 1996; Vol. 33.

(5) Kaim, W.; Schwederski, B. *Bioinorganic Chemistry: Inorganic Elements in the Chemistry of Life: An Introduction and Guide*; Wiley: Chichester and New York, 1994.

(6) Rothemund, P. W. K. *Nature* **2006**, *440*, 297.

(7) Sivakova, S.; Rowan, S. J. *Chem. Soc. Rev.* **2005**, *34*, 9.

(8) Tanaka, K.; Tengeiji, A.; Kato, T.; Toyama, N.; Shionoya, M. *Science* **2003**, *299*, 1212.

(9) Lippert, B. *Coord. Chem. Rev.* **2000**, *200/202*, 487.

(10) Cerda, B. A.; Wesdemiotis, C. *J. Am. Chem. Soc.* **1996**, *118*, 11884.

(11) Rodgers, M. T.; Armentrout, P. B. *J. Am. Chem. Soc.* **2000**, *122*, 8548.

(12) Rodgers, M. T.; Armentrout, P. B. *J. Am. Chem. Soc.* **2002**, *124*, 2678.

(13) Yang, Z. B.; Rodgers, M. T. *J. Phys. Chem. A* **2006**, *110*, 1455.

(14) Yang, Z.; Rodgers, M. T. *Int. J. Mass Spectrom.* **2005**, *241*, 225.

(15) Yang, Z.; Rodgers, M. T. *J. Am. Chem. Soc.* **2004**, *126*, 16217.

(16) Liu, H.; Sun, J. L.; Hu, Y.; Han, K. L.; Yang, S. *Chem. Phys. Lett.* **2004**, *389*, 342.

(17) Sun, J. L.; Liu, H.; Wang, H.-M.; Han, K. L.; Yang, S. *Chem. Phys. Lett.* **2004**, *392*, 285.

(18) Pedersen, D. B.; Simard, B.; Martinez, A.; Moussatova, A. *J. Phys. Chem. A* **2003**, *107*, 6464.

(19) Pedersen, D. B.; Zgierski, M. Z.; Denommee, S.; Simard, B. *J. Am. Chem. Soc.* **2002**, *124*, 6686.

(20) Pedersen, D. B.; Zgierski, M. Z.; Simard, B. *J. Phys. Chem. A* **2003**, *107*, 6457.

(21) Russo, N.; Toscano, M.; Grand, A. *J. Am. Chem. Soc.* **2001**, *123*, 10272.

(22) Russo, N.; Toscano, M.; Grand, A. *J. Mass Spectrom.* **2003**, *38*, 265.

(23) Burda, J. V.; Sponer, J.; Hobza, P. *J. Phys. Chem.* **1996**, *100*, 7250.

(24) Noguera, M.; Bertran, J.; Sodupe, M. *J. Phys. Chem. A* **2004**, *108*, 333.

(25) Burda, J. V.; Sponer, J.; Leszczynski, J.; Hobza, P. *J. Phys. Chem. B* **1997**, *101*, 9670.

(26) Martinez, A. *J. Chem. Phys.* **2005**, *123*, 024311.

(27) Moussatova, A.; Vazquez, M. V.; Martinez, A.; Dolgounitcheva, O.; Zakrzewski, V. G.; Ortiz, J. V.; Pedersen, D. B.; Simard, B. *J. Phys. Chem. A* **2003**, *107*, 9415.

(28) Vazquez, M.-V.; Moussatova, A.; Martinez, A.; Dolgounitcheva, O.; Zakrzewski, V. G.; Ortiz, J. V. *J. Phys. Chem. A* **2004**, *108*, 5845.

(29) Kumar, A.; Mishra, P. C.; Suhai, S. *J. Phys. Chem. A* **2006**, *110*, 7719.

(30) Rothschopf, G. K.; Perkins, J. S.; Li, S.; Yang, D. S. *J. Phys. Chem. A* **2000**, *104*, 8178.

(31) Proch, D.; Trickl, T. *Rev. Sci. Instrum.* **1989**, *60*, 713.

(32) Moore, C. E. *Atomic Energy Levels*; National Bureau of Standards: Washington, DC, 1971.

(33) Sohnlein Bradford, R.; Yang, D. S. *J. Chem. Phys.* **2006**, *124*, 134305.

(34) Frisch, M. J.; Trucks, G. W.; Schlegel, H. B.; Scuseria, G. E.; Robb, M. A.; Cheeseman, J. R.; Montgomery, J. A., Jr.; Vreven, T.; Kudin, K. N.; Burant, J. C.; Millam, J. M.; Iyengar, S. S.; Tomasi, J.; Barone, V.; Mennucci, B.; Cossi, M.; Scalmani, G.; Rega, N.; Petersson, G. A.; Nakatsuji, H.; Hada, M.; Ehara, M.; Toyota, K.; Fukuda, R.; Hasegawa, J.; Ishida, M.; Nakajima, T.; Honda, Y.; Kitao, O.; Nakai, H.; Klene, M.; Li, X.; Knox, J. E.; Hratchian, H. P.; Cross, J. B.; Bakken, V.; Adamo, C.; Jaramillo, J.; Gomperts, R.; Stratmann, R. E.; Yazyev, O.; Austin, A. J.; Cammi, R.; Pomelli, C.; Ochterski, J. W.; Ayala, P. Y.; Morokuma, K.; Voth, G. A.; Salvador, P.; Dannenberg, J. J.; Zakrzewski, V. G.; Dapprich, S.; Daniels, A. D.; Strain, M. C.; Farkas, O.; Malick, D. K.; Rabuck, A. D.; Raghavachari, K.; Foresman, J. B.; Ortiz, J. V.; Cui, Q.; Baboul, A. G.; Clifford, S.; Cioslowski, J.; Stefanov, B. B.; Liu, G.; Liashenko, A.; Piskorz, P.; Komaromi, I.; Martin, R. L.; Fox, D. J.; Keith, T.; Al-Laham, M. A.; Peng, C. Y.; Nanayakkara, A.; Challacombe, M.; Gill, P. M. W.; Johnson, B.; Chen, W.; Wong, M. W.; Gonzalez, C.; Pople, J. A. *GAUSSIAN 03*, revision C.02; Gaussian, Inc.: Wallingford, CT, 2004.

(35) Berces, A.; Zgierski, M. Z.; Yang, D.-S. *Computational Molecular Spectroscopy*; Wiley: New York, 2000; p 110.

(36) Yang, D.-S.; Zgierski, M. Z.; Rayner, D. M.; Hackett, P. A.; Martinez, A.; Salahub, D. R.; Roy, P.-N.; Carrington, T., Jr. *J. Chem. Phys.* **1995**, *103*, 5335.

(37) Duschinsky, F. *Acta Physicochim. URSS* **1937**, *7*, 551.

(38) Rejnek, J.; Hanus, M.; Labelac, M.; Ryjacek, F.; Hobza, P. *Phys. Chem. Chem. Phys.* **2005**, *7*, 2006.

(39) Kryachko, E. S.; Nguyen, M. T.; Zeegers-Huyskens, T. *J. Phys. Chem. A* **2001**, *105*, 1288.

(40) Colarusso, P.; Zhang, K.; Guo, B.; Bernath, P. F. *Chem. Phys. Lett.* **1997**, *269*, 39.

(41) Ivanov, A. Y.; Plokhotnichenko, A. M.; Radchenko, E. D.; Sheina, G. G.; Blagoi, Y. P. *J. Mol. Struct.* **1995**, *372*, 91.

(42) Szczesniak, M.; Nowak, M. J.; Rostkowska, H.; Szczepaniak, K.; Person, W. B.; Shugar, D. *J. Am. Chem. Soc.* **1983**, *105*, 5969.

(43) Hobza, P.; Sponer, J. *Chem. Rev.* **1999**, *99*, 3247.

(44) Estrin, D. A.; Paglieri, L.; Corongiu, G. *J. Phys. Chem.* **1994**, *98*, 5653.

(45) Chin, S.; Scott, I.; Szczepaniak, K.; Person, W. B. *J. Am. Chem. Soc.* **1984**, *106*, 3415.

(46) Wang, X.; Lee, J. S.; Yang, D.-S. *J. Phys. Chem. A* **2006**, *110*, 12777.

(47) Sohnlein, B. R.; Li, S.; Fuller, J. F.; Yang, D.-S. *J. Chem. Phys.* **2005**, *123*, 014318.

(48) Yang, D. S.; Zgierski, M. Z.; Hackett, P. A. *J. Chem. Phys.* **1998**, *108*, 3591.

(49) Yang, D. S.; Zgierski, M. Z.; Berces, A.; Hackett, P. A.; Roy, P. N.; Martinez, A.; Carrington, T.; Salahub, D. R.; Fournier, R.; Pang, T.; Chen, C. F. *J. Chem. Phys.* **1996**, *105*, 10663.

(50) Lide, D. R.; Frederikse, H. P. R. *CRC Handbook of Chemistry and Physics*, 78th ed.; CRC: New York, 1997.